HHS Public Access

Author manuscript

Cell Rep. Author manuscript; available in PMC 2021 April 15.

Published in final edited form as:

Cell Rep. 2021 March 16; 34(11): 108866. doi:10.1016/j.celrep.2021.108866.

High dietary salt amplifies osmoresponsiveness in vasopressin-releasing neurons

David I. Levi[1,4,5], **Joshua C. Wyrosdic**[1,4], **Amirah-Iman Hicks**[3], **Mary Ann Andrade**[2], **Glenn M. Toney**[2], **Masha Prager-Khoutorsky**[3,*], **Charles W. Bourque**[1,6,*]

[1]Brain Repair and Integrative Neuroscience Program, Research Institute of the McGill University Health Centre, Montreal General Hospital, 1650 Cedar Avenue, Montreal, QC H3G1A4, Canada

[2]Department of Cellular and Integrative Physiology, University of Texas Health Sciences Centre San Antonio, 7703 Floyd Curl Drive, San Antonio, TX 78229, USA

[3]Department of Physiology, McGill University, 3644 Promenade Sir William Osler, Montreal, QC H3G1Y6, Canada

[4]These authors contributed equally

[5]Present address: Faculty of Medicine, Université de Montréal, 2900 Edouard Montpetit Blvd, Montreal, QC H3T1J4, Canada

[6]Lead contact

SUMMARY

High dietary salt increases arterial pressure partly through activation of magnocellular neurosecretory cells (MNC^{VP}) that secrete the antidiuretic and vasoconstrictor hormone vasopressin (VP) into the circulation. Here, we show that the intrinsic and synaptic excitation of MNC^{VP} caused by hypertonicity are differentially potentiated in two models of salt-dependent hypertension in rats. One model combined salty chow with a chronic subpressor dose of angiotensin II (AngII-salt), the other involved replacing drinking water with 2% NaCl (salt loading, SL). In both models, we observed a significant increase in the quantal amplitude of EPSCs on MNC^{VP}. However, model-specific changes were also observed. AngII-salt increased the probability of glutamate release by osmoreceptor afferents and increased overall excitatory network drive. In contrast, SL specifically increased membrane stiffness and the intrinsic

*Correspondence: masha.prager-khoutorsky@mcgill.ca (M.P.-K.), charles.bourque@mcgill.ca (C.W.B.).

AUTHOR CONTRIBUTIONS

D.I.L., J.C.W., G.M.T., M.P.-K., and C.W.B. designed the experiments. D.I.L. and J.C.W. performed osmotic minipump surgeries related to Fos and *in vitro* electrophysiology experiments. M.A.A. performed osmotic minipump and telemetry device surgeries, as well as acute testing of V1 antagonist effects on arterial pressure. M.A.A. and G.M.T. analyzed all *in vivo* arterial pressure data. A.-I.H. and J.C.W. performed anti-fos immunostaining and related image acquisition. J.C.W. performed all the anti-fos image analysis. D.I.L. performed and analyzed all *in vitro* slice electrophysiology experiments. J.C.W. performed and analyzed all experiments on acutely isolated neurons including actin and tubulin staining, electrophysiology, volume analysis, and SICM experiments. Figures were prepared by D.I.L., J.C.W., and C.W.B. The paper was written by D.I.L and J.C.W. in consultation with C.W.B.

DECLARATION OF INTERESTS

The authors declare no competing interests.

SUPPLEMENTAL INFORMATION

Supplemental Information can be found online at https://doi.org/10.1016/j.celrep.2021.108866.

osmosensitivity of MNC^{VP}. These results reveal that dietary salt increases the excitability of MNC^{VP} through effects on the cell-autonomous and synaptic osmoresponsiveness of MNC^{VP}.

In brief

Levi et al. show that rats subjected to two distinct models of salt-dependent hypertension feature an increase in the osmoresponsiveness of neurosecretory neurons that release the antidiuretic and vasoconstrictor hormone vasopressin. However, this common effect is associated with different cellular and synaptic changes that characterize each of the models.

Graphical Abstract

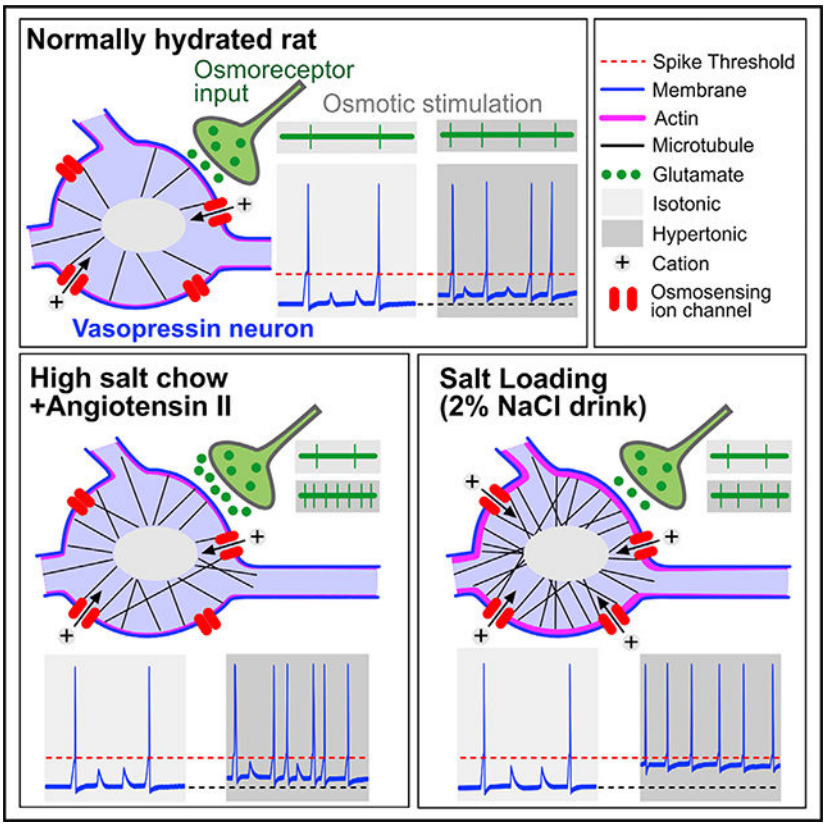

INTRODUCTION

High dietary salt intake is a well-established factor in the pathogenesis of hypertension; however, the mechanisms by which salt increases mean arterial pressure (MAP) remain poorly understood (Malta et al., 2018). Previous work has shown that high salt intake can increase vasoconstriction and MAP through a centrally driven increase in sympathetic tone (Boegehold, 2002; Brown et al., 1999; Fink et al., 2000; King et al., 2007; Kuroki et al., 2012; McBryde et al., 2007; Xu et al., 2007). The neural drive for this effect originates specifically from neurons in the organum vasculosum lamina terminalis (OVLT) (Kinsman et al., 2017b; Kinsman et al., 2017c; Nomura et al., 2019; Shi et al., 2007; Toney and Stocker, 2010), which comprises sodium(Na^+) and osmo-sensitive neurons that are excited

by increases in extracellular fluid osmolality or Na^+ concentration (Ciura and Bourque, 2006; Gizowski and Bourque, 2020; Kinsman et al., 2017a; Nissen et al., 1993; Nomura et al., 2019; Vivas et al., 1990). Experiments *in vivo* have shown that OVLT neurons can increase sympathetic drive through a polysynaptic circuit that includes neurons in the hypothalamic paraventicular nucleus (PVN) and preautonomic neurons in the rostral ventrolateral medulla (RVLM) (Basting et al., 2018; Fujita and Fujita, 2016; Nomura et al., 2019; Osborn et al., 2007; Shi et al., 2007; Son et al., 2013). However, pharmacological blockade of sympathetic tone does not completely reverse the hypertensive effect of high salt intake (Nomura et al., 2019), indicating that additional mechanisms contribute to the enhancement of MAP.

Recent work has shown that a significant fraction of the enhanced MAP associated with high salt intake in rats and mice is mediated by an increase in circulating levels of arginine vasopressin (VP) and activation of VP V_1 receptors (V_1R) in the periphery (Choe et al., 2015; Kim et al., 2013; Nomura et al., 2019). VP is a vasoconstrictor and antidiuretic hormone released by the axon terminals of hypothalamic magnocellular neurosecretory cells (MNCs) that project to the neurohypophysis. VP release into the bloodstream is triggered in proportion to the rate of action potentials initiated at their somata in the PVN and supraoptic nucleus (SON) (Bicknell, 1988; Bourque, 1991). Subjecting rats to a salt-loading (SL) protocol, where 2% NaCl is provided as drinking solution for 7 days, increases the electrical activity of VP-releasing MNCs (MNC^{VP}) *in vivo* (Choe et al., 2015), thereby explaining the high VP levels and V_1R-dependent increase in MAP after SL.

The mechanisms by which SL increases the firing rate of MNC^{VP} are not fully understood. Chronic high salt intake increases intracellular Cl^- and thus impairs the inhibitory effect of GABA (γ-amino butyric acid) on MNC^{VP} (Kim et al., 2011; Kim et al., 2013). Although this effect blunts the feedback from arterial baroreceptors that would normally dampen VP release as MAP rises (Choe et al., 2015), the activity of MNC^{VP} *in vivo* reflects a balance of the converging excitation by osmoreceptors and inhibition by baroreceptors (Kannan and Yagi, 1978; Leng et al., 2001). Therefore, the increased activity of MNC^{VP} caused by high salt intake could also involve a potentiation of the excitatory effects of systemic hypertonicity. Hypertonic conditions depolarize MNC^{VP} through the activation of ΔN-Trpv1 cation channels encoded by the transient receptor potential vanilloid 1 gene (Sharif Naeini et al., 2006; Sudbury et al., 2010; Zaelzer et al., 2015), and action potential firing is further promoted by an increase in the AMPA receptor-dependent excitatory synaptic drive they receive from OVLT neurons (Richard and Bourque, 1995; Trudel and Bourque, 2010). The objective of this study was to compare the osmoresponsiveness of MNC^{VP} in rats subjected to two distinct models of salt-dependent hypertension that feature different levels of serum osmolality during the hypertensive phase of the treatment. Our results show that osmoresponsiveness is sensitized in both models but with model-specific effects.

RESULTS

Rats were either kept euhydrated (EU) or subjected to one of two high salt intake protocols known to promote salt-dependent hypertension: the *SL model* (2% NaCl as drinking fluid for 7 days; Figure 1A; raw data in Data S1) (Choe et al., 2015; Kim et al., 2013), or the

AngII-salt model (4% sodium chow for 5 weeks combined with subcutaneous delivery of a subpressor dose of Angiotensin II during weeks 4 and 5; Figure 1B, King and Fink, 2006). Mean values (±SEM) of serum osmolality were 339 ± 3 mosmol/kg after SL (n = 61) and 302 ± 1 mosmol/kg after AngII-salt (n = 32). Only the SL group displayed a statistically significant increase in serum osmolality compared to EU (EU 299 ± 1 mosmol/kg; n = 18, $p < 0.001$, H = 72.6; one-way ANOVA on ranks and Dunn's post hoc test; Figure 1C).

The SL model is known to induce a hypertension that depends in part on peripheral V_1Rs (Choe et al., 2015; Kim et al., 2013), but it is unknown whether the increase in MAP induced by AngII-salt features a VP-dependent component. To address this issue, rats instrumented with blood pressure telemetry were maintained on normal chow and water for 5 weeks (EU) or subjected to the AngII-salt protocol (Figure 1B). As shown in Figure 1D, MAP was significantly higher following AngII-salt treatment (157 ± 4 mmHg, n = 7) compared to before treatment (103 ± 2 mmHg, n = 7; $p < 0.0000118$, paired t test), whereas MAP in EU rats was not different before (94 ± 2 mmHg,n = 6) or after the 5-week period (101 ± 2 mmHg, n = 6; $p = 0.0977$, paired t test). The contribution of V_1Rs to the maintenance of MAP was determined by examining the effects of injecting the V_1R antagonist H-3186 (Phenylac1, D-Tyr(Et)2, Lys6, Arg8, des-Gly9)-VP; 5.5 μg/kg i.v.; Figure S1). As shown in Figure 1E, the decrease in MAP induced by H-3186 was significantly greater in AngII-salt (−6.9 ± 2.2 mmHg; n = 6) than EU animals (0.3± 0.8 mmHg; n = 5; $p = 0.02$, t test). Therefore, animals subjected to either AngII-salt or SL develop hypertension that is in part mediated by peripheral V_1Rs.

AngII-salt and SL sensitize osmoresponsiveness of MNC^{VP} *in vivo*

To determine whether AngII-salt and SL enhance the osmoresponsiveness of MNC^{VP} compared to EU, we examined the effect of injecting hypertonic saline (HS, 2M NaCl, 1.43 mL/kg, s.c.), or vehicle (0.15 M NaCl, isotonic saline) on the percentage of SON MNC^{VP} expressing c-*fos* in animals subjected to each treatment (Figures 2A–2C). A nonparametric analysis of the data confirmed the presence of significant differences between these groups ($p < 0.0001$, Kruskal-Wallis test), and comparisons between pairs of groups were subsequently performed using nonparametric t tests (Mann-Whitney). Although injection of HS significantly increased the percentage of MNC^{VP} expressing c-*fos* in all treatments (EU $p = 0.0007$; SL $p = 0.0043$; AngII-salt $p = 0.0022$), the percentage of MNC^{VP} expressing c-*fos* following HS injection was significantly greater in rats treated with SL ($p = 0.0016$) and AngII-salt ($p = 0.0007$) compared to EU (Figure 2C), suggesting that the excitatory effect of HS on MNC^{VP} is enhanced by these treatments.

High dietary salt increases membrane conductance in MNC^{VP}

To examine whether the electrical properties of VP releasing neurons are affected by these treatments, SON neurons identified as MNC^{VP} by expression of eGFP (Ueta et al., 2005) were analyzed using patch-clamp recording in angled horizontal brain slices that retain OVLT-SON connectivity (Figures S2A and S2B). According to Ohm's law the amplitude of voltage responses to current generated by ion channels varies inversely with input conductance when evoked from the same voltage. To determine whether SL and AngII-salt treatments affect input conductance, MNC^{VP} were subjected to 500 ms voltage steps (V_H =

−60 mV; Figure S2C), and input conductance was determined from the slope of the linear part of the current-voltage plot (−80 to −60 mV). As shown in Figure S2D, the average input conductance of MNC^{VP} recorded in slices prepared from animals subjected to both treatments was significantly greater than EU (EU 2.14 ± 0.09 nS versus SL 2.94 ± 0.12 nS, $p < 0.001$; AngII-salt 2.63 ± 0.13 nS, $p = 0.003$; $F = 14.8$, one-way ANOVA and Holm-Sidak post hoc test). Therefore, based on Ohmic principles alone, MNC^{VP} in SL and AngII-salt animals should be less responsive to currents generated by ΔN-Trpv1 and synaptically activated AMPA receptors.

SL and AngII-salt increase osmoresponsiveness of MNC^{VP} *in vitro*

To determine whether SL and AngII-salt treatments alter the electrical osmoresponsiveness of MNC^{VP}, we examined the effects of a bath application of a hypertonic stimulus (15 mM mannitol) for 10 min during whole-cell current-clamp recordings. As shown in Figures 3A–3C, hyperosmotic stimulation significantly increased the action potential firing rate of neurons recorded from slices prepared from rats subjected to all treatments (EU from 2.8 ± 0.8 to 3.7 ± 0.7 Hz, $n = 13$, $p = 0.01$; SL from 2.1 ± 0.7 to 5.9 ± 0.4 Hz, $n = 13$, $p = 0.00057$; AngII-salt from 3.5 ± 0.6 to 6.1 ± 0.4 Hz, $n = 19$, $p = 0.00001$; paired t tests), and this effect was associated with a significant depolarization of the membrane potential (EU from −48.0 to −46.3 mV, $p = 0.02$; SL from −47.1 to −42.6 mV, $p = 0.001$; AngII-salt from −46.7 to −44.5 mV, $p = 0.021$; paired t test). However, the average increase in firing rate induced by hypertonicity was significantly greater in SL (+3.7 ± 0.8 Hz) and AngII-salt (+2.6 ± 0.4 Hz) compared with EU (+0.9 ± 0.3 Hz; $H = 10.8$; $p = 0.004$; one-way ANOVA on ranks and Dunn's post hoc test; Figure 3D). Although the average hypertonicity-induced depolarization was not significantly different across conditions when tested by ANOVA (EU +1.77 ± 0.65 mV; SL +4.42 ± 1.03 mV; AngII-salt +2.14 ± 0.83 mV; $F = 2.584$, $p = 0.088$), the average depolarization recorded in SL appeared greater than EU, and this difference was significant when compared by t test ($p = 0.043$, Figure 3E), whereas a t test comparison of the depolarization observed in EU and AngII-salt was not significant ($p = 0.745$). These results indicate that despite their higher input conductance, MNC^{VP} display enhanced responsiveness to hypertonic stimulation in SL and AngII-salt conditions, and that an increase in the intrinsic osmosensitivity of MNC^{VP} might contribute to this sensitization in SL but not in AngII-salt animals.

Ang-salt treatment increases synaptic excitation of MNC^{VP}

To determine whether high dietary salt intake affects synaptic excitation of MNC^{VP} by osmosensory afferents, we first compared changes in spontaneous EPSC (sEPSC) frequency induced by hyperosmotic stimulation in the presence of 5 μM bicuculline to block inhibitory currents mediated by $GABA_A$ receptors. Bath application of 15 mM mannitol significantly increased sEPSC frequency in all conditions (EU, from 1.89 ± 0.23 to 2.49 ± 0.29 Hz; $n = 14$, $p = 0.00017$; SL from 2.01 ± 0.09 to 2.62 ± 0.18 Hz; $n = 13$, $p = 0.0015$; AngII-salt from 3.18 ± 0.45 to 4.34 ± 0.55 Hz; $n = 17$, $p = 0.000003$; paired t tests; Figures 4A–4C). Whereas the mean increase in sEPSC frequency induced by hyperosmolality was not different between EU (+0.60 ± 0.12 Hz) and SL (+0.61 ± 0.15 Hz), the response observed in AngII-salt was significantly greater than in both EU and SL preparations (+1.16 ± 0.17 Hz, $F = 4.81$, $p = 0.032$ [EU] and $p = 0.026$ [SL]; one-way ANOVA and Holm-Sidak post hoc

test; Figure 4D). Although average sEPSC amplitudes in SL (−22.5 ± 0.9 pA) and AngII-salt (−22.1 ± 1.2 pA) appeared larger than in EU (−19.6 ± 0.9 pA), this effect was not statistically significant ($p = 0.068$, Kruskal-Wallis one-way ANOVA on ranks; Figure 4E).

SL and AngII-salt treatments increase EPSC quantal size

To determine whether SL and AngII-salt cause changes in the strength of excitatory synapses, we examined how these treatments affect the amplitude of quantal excitatory events. As shown in Figures 5A–5C, the amplitudes of miniature EPSCs (mEPSCs) recorded in the presence of 5 μM bicuculline and 1 μM tetrodotoxin were significantly increased by both treatments (EU −14.4 ± 0 0.6 pA versus SL −23.4 ± 1.0 pA and AngII-salt −19.2 ± 1.5 pA; $p < 0.001$, $H = 27.3$, Kruskal-Wallis one-way ANOVA on ranks and Dunn's post hoc test). To examine whether quantal size is specifically enhanced at excitatory synapses in the OVLT→SON pathway, we examined the amplitude of asynchronous EPSCs (aEPSCs) detected after the compound EPSC evoked by electrical stimulation of the OVLT (Iremonger and Bains, 2007; Stachniaketal.,2014; Trudel and Bourque,2010).As shown in Figures 5D–5F, the amplitudes of aEPSCs were also significantly increased by both treatments (EU −20.7 ± 1.5 pA versus SL −28.5 ± 2.1 pA and AngII-salt −28.6 ± 2.2 pA; $p < 0.05$, $F = 4.74$, one-way ANOVA and Holm-Sidak post hoc test).

AngII-salt treatment increases probability of release (P_r) at glutamatergic synapses

The amplified osmotically evoked increase in sEPSC frequency observed in AngII-salt (Figure 4D) could have resulted from an increase in P_r at glutamatergic synapses on MNC^{VP}, or to an increase in the number of glutamatergic synapses on these neurons. Indeed, the frequency of mEPSCs, which varies in proportion to P_r and synapse number, was significantly higher in AngII-salt (2.7 ± 0.3 Hz) compared to the other conditions (EU, 1.6 ± 0.1 Hz; SL, 2.1 ± 0.2 Hz; $H = 8.39$, $p = 0.015$, Kruskal-Wallis one-way ANOVA on ranks and Dunn's post hoc test; Figure 5B). Similarly, the frequency of aEPSCs elicited by electrical stimulation of the OVLT was significantly greater in AngII-salt (40.0 ± 1.7 Hz) compared to the other conditions (EU, 31.7 ± 2.8 Hz; SL, 26.1 ± 2.6 Hz; $F = 9.58$, $p < 0.001$, one-way ANOVA and Holm-Sidak post hoc test; Figure 5E).

To determine whether changes in P_r specifically contributed to these effects, we also examined the impact of SL and AngII-salt on the paired pulse ratio ($PPR = EPSC_2/EPSC_1$) calculated from the charge transfer that occurred during EPSCs evoked by a pair of electrical stimuli delivered to the OVLT 50 ms apart (Figure 5G). The PPR reflects the degree of short-term facilitation caused by the presence of residual Ca^{2+} in the presynaptic terminal at the time of pulse 2, and conditions that reduce PPR are indicative of increased P_r (Zucker and Regehr, 2002). As illustrated in Figure 5H, the degree of facilitation observed during pulse 2 was lower in cells from AngII-salt preparations, and the average value of PPR was significantly lower in this group (1.66 ± 0.04, $n = 15$) compared to either EU (1.93 ± 0.08, $n = 12$, $p = 0.016$) or SL (1.98 ± 0.08, $n = 13$; $p = 0.004$; $F = 6.89$, one-way ANOVA and Holm-Sidak post hoc test; Figure 5I).

SL increases mechanosensitivity in MNC^{VP}

Recordings from MNC^{VP} in slices suggested that the intrinsic osmosensitivity of these cells may be enhanced by SL (Figure 3E). The osmosensitivity of MNC^{VP} reflects a mechanical activation of ΔN–Trpv1 cation channels during cell shrinking, and this response requires an intact subcortical network of filamentous actin (F-actin) and a dense scaffold of microtubules (Prager-Khoutorsky and Bourque, 2010; Prager-Khoutorsky et al., 2014; Zaelzer et al., 2015; Zhang et al., 2007). To examine whether the cell-autonomous mechanosensitivity of MNC^{VP} is affected by chronic high salt intake, we examined the effects of SL and AngII-salt on neurons acutely isolated from the SON of adult rats. Isolated MNC^{VP} were identified by the expression of eGFP (Figure6A) and recorded under whole-cell current clamp. To determine whether the mechanosensitivity of the neurons was affected by chronic high salt intake, negative pressure (−30 mmHg) was applied to the recording pipette to cause cell shrinking and induce a mechanosensory response. Membrane voltage was recorded continuously, and phase-contrast images were captured at 0.5 Hz. The effects of the stimulus on cell volume, membrane potential, and action potential firing were measured once the cell had undergone a visible amount of shrinking (≥2%). As illustrated in Figure 6B, the excitatory effect of the mechanical stimulus was more pronounced in cells obtained from SL-treated rats than either EU or AngII-salt. Indeed, the change in firing rate evoked by negative pressure was greater in SL (+4.7 ± 1.6 Hz, n = 12 from 9 animals) compared to EU (+1.2 ± 0.5 Hz, n = 13 from 8 animals) or AngII-salt (+1.6 ± 1.0Hz, n = 11 from5 animals; $p = 0.005$; one-way ANOVA on ranks and Dunn's post hoc test; Figure 6C). Similarly, the average depolarization caused by negative pressure was greater in SL (+17.2 ± 3.2 mV, n = 12) than either EU (+5.6 ± 1.6 mV, n = 12) or AngII-salt (+7.4 ± 2.7 mV, n = 10, $p = 0.004$; one-way ANOVA on ranks and Dunn's post hoc test; Figure 6D). Interestingly, the enhanced response of SL-treated MNC^{VP} occurred despite a significantly smaller degree of shrinking (SL 7.1% ± 0.8%) compared with either EU (10.4% ± 2.5%) or AngII-salt (10.0% ± 1.1%; $F = 4.422$; $p = 0.021$, one-way ANOVA and Student-Newman-Keuls post hoc test; Figure 6E).

SL increases cytoskeletal density and membrane stiffness in MNC^{VP}

The reduced shrinking response of MNC^{VP} to negative pressure applied via the patch pipette suggests that the SL treatment may have caused an increase in cell stiffness. Since F-actin and microtubules are key structural elements that determine cell stiffness (Brangwynne et al., 2006; Gardel et al., 2004a; Shin et al., 2004) and mediate mechanical activation of ΔN-Trpv1 channels (Prager-Khoutorsky and Bourque, 2015), we examined whether the density of these cytoskeletal elements was increased by SL. As shown in Figures 7A and 7B, the subcortical region of MNC^{VP} labeled with fluorescent phalloidin, which selectively binds F-actin, was significantly brighter in MNC^{VP} from SL rats (n = 101 from 3 animals) compared to EU (n = 100 from 3 animals) or AngII-salt (n = 103 from 5 animals) ($p < 0.001$, $H = 77.0$; Kruskal-Wallis one-way analysis of variance on ranks and Dunn's post hoc test). Similarly, the cytoplasm of MNC^{VP} labeled with anti-α-tubulin antibody was significantly brighter in MNC^{VP} from SL rats (n = 84 from 3 animals) compared to EU (n = 92 from 3 animals) or AngII-salt (n = 77 from 3 animals) ($p < 0.001$, $H = 47.6$; Kruskal-Wallis one-way analysis of variance on ranks and Dunn's post hoc test; Figures 7C and 7D; Figure S3).

To determine whether SL increases the rigidity of identified isolated MNC^{VP}, pressure-distance curves were measured at the surface of the cells using a scanning ion conductance microscope (SICM) (Pellegrino et al., 2012). The SICM probe (18 MΩ saline-filled pipette) was advanced to the cell surface until a stable z-Piezo position was detected. A slow pressure ramp was then applied to the recording pipette (~2 mmHg/s) to cause a progressive increase in outwardly directed saline flow at the tip of the probe (Figure 7E). The SICM maintains a constant gap between the probe's tip and the receding cell surface and provides a high-resolution (0.02 nm) readout of z-Piezo displacement as pressure rises in the pipette (Figure 7F). As illustrated in Figures 7G and 7H, the slope of the z-Piezo versus pipette pressure relation was significantly smaller in MNC^{VP} from SL rats (−31.5 ± 7.1 nm/mmHg, n = 12 from 5 animals) compared to both EU (−81.6 ± 13.8 nm/mmHg, n = 11 from 8 animals, p = 0.011) and AngII-salt (−73.0 ± 14.3 nm/mmHg, n = 9 from 3 animals, p = 0.039; F = 5.64; one-way ANOVA and Holm-Sidak post hoc test).

DISCUSSION

Osmoresponsiveness of MNC^{VP} is enhanced by SL and AngII-salt

VP released by the axon terminals of MNC^{VP} has recently emerged as a significant contributing factor in the pathogenesis of salt-dependent hypertension (Prager-Khoutorsky et al., 2017). Although pharmacological blockade of peripheral V_1Rs does not affect blood pressure at rest in healthy rats (Palmer, 2015), such receptors mediate a significant portion of the increase in MAP observed in animals subjected to SL (Choe et al., 2015) and deoxycorticosterone acetate (DOCA)-salt (Kim et al., 2013). Our experiments reveal that a significant component of the increased MAP resulting from AngII-salt treatment is also mediated by V_1Rs. Therefore, it has become increasingly important to determine the factors by which high salt intake can promote VP release.

Previous work has shown that MNC^{VP} in rats subjected to SL or DOCA-salt display an accumulation of intracellular chloride that impairs $GABA_A$ receptor-mediated hyperpolarization and inhibition mediated by arterial baroreceptors (Choe et al., 2015; Kim et al., 2013). Loss of negative feedback from baroreceptors may promote the activation of MNC^{VP} by enhancing the ratio of excitation to inhibition following such treatments. However, this effect could be further amplified by a strengthening of osmotically induced excitatory mechanisms. We found that systemic HS induces expression of the activity-dependent protein c-*fos* in a significantly greater proportion of SON MNC^{VP} in AngII-salt and SL rats than in EU animals (Figure 2). The c-*fos* protein is transiently expressed in response to an acute rise of intracellular calcium, suggesting that the excitatory effect of the osmotic stimulus was greater in treated animals. Interestingly, levels of c-*fos* expression were not significantly different in vehicle-treated animals across the three groups, despite evidence that the spontaneous electrical activity of MNC^{VP} is higher in salt-treated animals (Choe et al., 2015). This observation presumably reflects the fact that treatments such as SL cause a slow and gradual increase in the electrical activity of MNC^{VP} (i.e., over several days), allowing the auto-inhibitory effect of c-*fos* on its own expression to blunt changes in basal expression (Chung, 2015).

In agreement with our observations *in vivo*, the excitatory effect of acute hyperosmolality on MNC^{VP} was enhanced in cells recorded *in vitro*, in slices obtained from animals subjected to either SL or AngII-salt treatment. Because the increase in action potential firing observed in MNC^{VP} exposed to an acute hypertonic stimulus reflects the combined effect of increased synaptic excitation by glutamatergic afferents from the OVLT and the membrane depolarization caused by the activation of non-selective cation channels during cell shrinking (Bourque, 2008), we examined whether these processes were equally affected by both treatments.

AngII-salt and SL strengthen OVLT→MNC^{VP} synapses

Analysis of quantal excitatory synaptic events revealed pre- and post-synaptic changes that would promote excitation of MNC^{VP} in animals subjected to both SL and AngII-salt. Notably, the amplitudes of mEPSCs were significantly enhanced by both SL and AngII-salt, suggesting that these treatments cause an increase in the density of postsynaptic AMPA receptors at glutamatergic synapses onto MNC^{VP}. Moreover, the amplitudes of aEPSC evoked by electrical stimulation of the OVLT were also significantly enhanced, indicating that OVLT→MNC^{VP} synapses were specifically potentiated postsynaptically. The increased postsynaptic amplitude of quantal currents is functionally important because it likely compensates for the increased input conductance of the cells and allows the generation of excitatory postsynaptic potentials capable of triggering action potentials. Although previous work has established that MNCs can undergo activity-dependent long-term potentiation (Panatier et al., 2006), the mechanisms by which AngII-salt and SL increase quantal size remain to be determined. Of note, changes in quantal size induced by SL and AngII-salt are sustained for many days and confer an adaptive positive feedback character that contributes to the sustained enhancement of electrical activity in chronically stimulated MNC^{VP}. As such, the synaptic changes induced by AngII-salt and SL are opposite to the relatively rapid autoregulatory decrease in synaptic gain that would be expected from homeostatic synaptic scaling (Keck et al., 2017). Why some synapses follow scaling rules but not others is an important matter that requires investigation.

In contrast to the postsynaptic enhancement of glutamatergic synapses that was observed following both forms of treatment, changes in the presynaptic compartment of excitatory synapses were only observed following AngII-salt. Indeed, whereas the frequency of mEPSCs and aEPSCs was unaffected by SL, frequencies of both types of events were increased in MNC^{VP} from rats treated with AngII-salt. An increase in the frequency of aEPSCs and mEPSCs reflects either an increase in P_r or an increase in the number of release sites being monitored (i.e., synapses). The observation that paired pulse facilitation at OVLT-MNC^{VP} synapses is reduced in slices from AngII-salt but not SL-treated animals confirms the absence of presynaptic changes in SL. Moreover, this result indicates that part of the increased aEPSC and mEPSC frequency observed in AngII-salt animals specifically reflects an increase in P_r at glutamatergic boutons, including those forming OVLT-MNC^{VP} synapses. The mechanism by which AngII-salt treatment increases P_r remains to be determined. Previous work has shown that locally applied AngII can acutely increase the frequency of mEPSCs (Ozaki et al., 2004). Moreover a recent study has shown that locally applied AngII can increase P_r at OVLT-MNC^{VP} synapses via release of nitric oxide from the post synaptic

cell (Stachniak et al., 2014), and the AngII derivative Ang^{1-7} has been shown to upregulate local nitric oxide synthase when injected into the hypothalamus (Cerrato et al., 2012). Further work is needed to define the signaling pathways by which AngII-salt enhances Pr at glutamatergic synapses on MNC^{VP}, and to determine whether new synapses are formed onto these neurons in response to such treatment.

Osmotically induced network activity is increased by AngII-salt but not SL

To determine whether glutamatergic network activity impinging on MNC^{VP} is affected by chronic high salt intake, we compared the changes in sEPSC frequency induced by an acute hypertonic stimulus in slices prepared from rats subjected to all conditions. We found that the increase in sEPSC frequency caused by a hypertonic stimulus in MNC^{VP} was significantly greater in slices prepared from rats subjected to AngII-salt compared to EU and SL (Figure 4). Previous work has shown that a large proportion of the sEPSCs detected in our recording conditions reflect action potential-dependent network activity originating from OVLT neurons (Trudel and Bourque, 2003, 2010). Therefore, the increased sEPSC response to a constant hyperosmotic stimulus observed after AngII-salt treatment could reflect either an increase in the action potential firing response of osmotically stimulated OVLT neurons that project to the SON, an increase in synapse number, or an increase in P_r at OVLT-MNC^{VP} glutamatergic synapses that would enhance the number of quanta released per action potential generated in the OVLT-MNC^{VP} pathway. Our observation that PPR is reduced in MNC^{VP} from AngII-salt animals indicates that an increase in P_r plays an important role in the enhancement of network excitation in this condition. Additional work is required to determine whether AngII-salt also increases the number of glutamatergic synapses on MNC^{VP} and/or the osmosensitivity of OVLT neurons.

Intrinsic osmosensitivity is increased by SL in MNC^{VP}

The excitation of MNC^{VP} in response to a hyperosmotic stimulus results from a combination of the increase in sEPSC frequency caused by activation of upstream OVLT neurons and the slow intrinsic depolarization produced by activation of ΔN-Trpv1 cation channels upon cell shrinking (Bourque, 2008). Our experiments showed that the depolarization of MNC^{VP} induced by hyperosmolality was greater in slices from SL rats when compared to EU using a t test (Figure 3E). To examine whether the effect of SL was associated with an increase in the cell-autonomous osmo-mechanical response of MNC^{VP}, we performed experiments on acutely isolated neurons. Whole-cell recordings showed that neurons subjected to the same amount of negative hydrostatic pressure applied through the recording pipette were significantly more depolarized and excited when cells were isolated from the SON of SL-treated rats compared to either EU or AngII-salt rats. Interestingly, the average amount of shrinking induced by a constant negative pressure stimulus was significantly smaller in neurons isolated from SL rats compared to EU, suggesting that MNC^{VP} are not only more mechanosensitive they are also mechanically stiffer in SL rats. When normalizing for volume change, the average excitatory effect of shrinking on neurons treated by SL was more than 5 times greater than EU.

The degree to which cells shrink in response to a decrease in internal hydrostatic pressure is determined by the tensile strength of the cytoskeleton and its ability to push against the

plasma membrane (Ingber, 2008). We therefore examined whether SL might cause an increase in the density of actin and tubulin, which are prominent cytoskeletal elements in MNC^{VP}. Imaging of identified cells stained with fluorescent phalloidin, or an antibody directed against α-tubulin, indicated that SL significantly increases signal intensity compared to EU. This observation is consistent with recent reports showing SL causes an increase in the density of these cytoskeletal components (Barad et al., 2020; Hicks et al., 2020). Indeed, pressure-distance analysis using SICM (Sánchez et al., 2008) confirmed the increased stiffness of MNC^{VP} in SL-treated rats. Our analysis was restricted to the force required to cause a membrane displacement of ~1 μm toward the interior of the cell from the resting position. This depth approximates the thickness of the subcortical F-actin layer in MNCs (Barad et al., 2020; Zhang and Bourque, 2008). In principle, the increased force required to cause this displacement in SL cells could reflect not only an increased density of F-actin within this layer but also an increase in the density or crosslinking of the underlying cytoskeletal scaffold due to tensigrity, including microtubules (Gardel et al., 2004b). Previous work has shown that microtubules project all the way to the plasma membrane in these cells, where they interact with the C terminus of ΔN-Trpv1 channels that they stimulate via push-activation during cell shrinking (Prager-Khoutorsky et al., 2014). However, MNC^{VP} isolated from rats treated with AngII-salt also displayed an increase in cytoplasmic α-tubulin, yet these cells did not show a significant increase in rigidity. These observations suggest that the resistance to physical movement of the plasma membrane that occurs in the immediate subcortical region is determined primarily by F-actin.

Previous work has shown that the integrity of the thin layer of F-actin beneath the plasma membrane is required for mechanosensitivity and osmosensitivity, and the gain of these responses scales in proportion with F-actin density (Prager-Khoutorsky and Bourque, 2010; Zhang and Bourque, 2008; Zhang et al., 2007). The observations that MNC^{VP} increase their mechanosensitivity and subcortical F-actin density when subjected to SL but not AngII-salt suggest these effects are not secondary consequences of enhanced MAP, which occurs in both. Rather, the increased subcortical F-actin density, membrane rigidity, and mechanosensitivity of MNC^{VP} may be a direct consequence of the chronic hyperosmotic stress, which is specific to the SL condition (Figure 1B). Whether the increased membrane rigidity contributes to the enhanced osmosensitivity of MNC^{VP} remains to be determined. Interestingly, SL treatment was previously shown to cause brain derived neurotrophic factor (BDNF)-dependent activation of TrkB (tropomyosin-related kinase B) receptors in MNCs (Choe et al., 2015), and TrkB receptors are known to engage pathways that can modulate actin and microtubule dynamics (Gonzalez et al., 2016). Further work is required to define the molecular mechanisms and signaling pathways by which AngII-salt and SL can differentially affect the synaptic and mechanosensitive regulation of MNC^{VP}, as well as any potential role of BDNF in the enhancement of osmosensitivity following SL treatment.

Concluding remarks

Systemic VP release has recently emerged as a causative factor in the pathogenesis of salt-dependent hypertension, and previous studies in rats treated with SL or DOCA-salt have indicated that a shift in excitatory/inhibitory (E/I) balance promoting activation of MNC^{VP} may be caused by impaired $GABA_A$ receptor-mediated inhibition (Choe et al., 2015; Kim et

al., 2013). In this study, we tested the hypothesis that high salt intake can cause a strengthening of excitatory mechanisms in these neurons. Our analysis revealed that the osmoresponsiveness of MNC^{VP} is significantly enhanced in two distinct models of salt-dependent hypertension: SL and AngII-salt. While both treatments caused a potentiation of quantal size at glutamatergic synapses, other changes were exclusively expressed in a single condition. AngII-salt caused an increased P_r in glutamatergic synapses on MNC^{VP}, whereas SL caused an increase in the cell-autonomous osmosensitivity of the cells. These findings indicate that chronic high dietary salt intake mediates a multitude of plastic changes within the brain that facilitate the excitation of MNC^{VP} and increase systemic VP release in a manner that can contribute to salt-dependent hypertension.

STAR⋆METHODS

RESOURCE AVAILABILITY

Lead contact—Further information and requests for resources and reagents should be directed to, and will be fulfilled by the Lead Contact, Charles W. Bourque (Charles.bourque@mcgill.ca).

Materials availability—This study did not generate new unique reagents.

Data and code availability—The raw data presented in the figures is provided in Data S1 in the supplementary information.

EXPERIMENTAL MODEL AND SUBJECT DETAILS

All procedures involving animals were performed according to protocol #AUP1190 and approved by the Facility Animal Care Committee (FACC) of McGill University, or the Institutional animal care and use committee of the University of Texas Health Science Center at San Antonio (UTHSCSA; protocol: 20100021AR). Experiments at McGill University were performed on in-house bred transgenic male Wistar rats (12–24 weeks) that express enhanced green fluorescent protein (eGFP) under the control of the *Avp* gene promoter (Ueta et al., 2005). Experiments at UTHSCSA were performed on adult male Sprague-Dawley rats (20–40 weeks; body weight: 400–450 g). Animals were housed under 12/12 h light/dark conditions (light 7AM-7PM), and food and water were provided *ad libitum*, except where specified.

SL-treated rats were provided with 2% NaCl solution as drinking fluid instead of water for 7 days as done previously (Choe et al., 2015). Animals subjected to the AngII-salt protocol were provided with chow containing 4% sodium chloride (D17013i, Research Diets Inc, New Brunswick, NJ,) for a period of 5 weeks. After the first 3 weeks the animals were anesthetized with isoflurane and implanted with a subcutaneous Osmotic Minipump (Alzet osmotic pumps, Cupertino CA) delivering Angiotensin II (Sigma Aldrich Ltd, St-Louis MO) at a rate of 150 ng/kg/min as described previously (Osborn et al., 2007). Animals remained on the high salt chow coupled with the minipump for the final 2 weeks. Previous work has shown that a steady state level of hypertension is reached 6 days after the onset of

Angiotensin II delivery in this model (King and Fink, 2006), therefore data were collected between days 32 and 35 of the protocol were included in the analysis.

METHODS DETAILS

Blood pressure monitoring—Development of AngII-salt hypertension was monitored by recording arterial blood pressure and heart rate (HR) in conscious unrestrained adult male Sprague-Dawley rats using radio telemetry as previously described (Osborn et al., 2007). To assess the effects of systemic V_1R blockade on MAP and HR, rats were anesthetized with a urethane (800 mg/kg)/α-chloralose (80 mg/kg) cocktail delivered by intraperitoneal injection. Catheters (PE-50 tubing) were implanted in a femoral artery and vein to record arterial pressure and administer drugs, respectively. HR was obtained from a lead I ECG. The trachea was cannulated, and rats were mechanically ventilated with oxygen-enriched room air. End-tidal CO_2 was monitored and maintained within a physiological range (5.0 ± 0.5%) by adjusting ventilation rate (85–95 breaths/min) and/or tidal volume (2–3 ml). Body temperature was maintained at 37 ± 1°C with a ventrally located water-circulating pad. Supplements of anesthetic (10% of the initial dose) were given when needed, as assessed by limb withdrawal to noxious foot pinch before paralysis and by a pressor response to foot pinch thereafter.

After recording stable baseline levels of arterial pressure and HR for ~20 minutes, the contribution of circulating VP to maintenance of MAP was determined in EU (n = 5) and AngII-salt (n = 6) rats by systemic blockade of V_1Rs by intravenous injection of the selective antagonist H-3186 (phenylac1, D-Tyr(et)2, Lys6, Arg8, des-Gly9)-VP).

c-fos analysis—Rats were injected with vehicle (0.15 M NaCl) or HS (2M NaCl) subcutaneously (s.c.) at a dose of 1.43 ml/kg. 1 hour later the animals were anesthetized with isoflurane and perfused with 4% paraformaldehyde. Brains were extracted and post-fixed by immersion for 48h then sectioned with a vibratome (50 μm thick) in the coronal plane. Sections were blocked with 10% normal goat serum (in phosphate buffered saline (PBS) containing 0.3% Triton-X and incubated overnight at 4°C with primary antibodies including rabbit polyclonal c-*fos* antibody (Millipore; 1:10,000) and PS41 anti-VP neurophysin mouse monoclonal antibody (1:50; provided by Dr. Hal Gainer, NIH). Following wash, sections were incubated for 1 hour with Alexa Fluor-conjugated secondary antibodies [405 and 568 nm; (Life Technologies; 1:500)], washed and mounted on glass slides. Z stacks of 10–13 confocal images were collected using a 20X objective on a confocal microscope (FV3000, Olympus Canada Inc., Richmond Hill, ON). All images were analyzed by an investigator blind to the treatment using ImageJ (v1.52p, NIH). Only cells that were clearly VP-positive and clearly c-*fos*-positive or -negative were counted to determine the percentage of VP cells expressing c-*fos* in each section. The percentage of c-*fos* positive MNC^{VP} in each animal was determined by averaging the values determined in 2–4 sections (number of MNC^{VP} in each section varied between 59 and 540).

Acute hypothalamic slices—Animals were euthanized by decapitation and trunk blood was collected to determine serum osmolality. Acute angled horizontal hypothalamic slices (400 μm thick) were prepared as described previously (Trudel and Bourque, 2010) and

placed in a recording chamber on a fixed-stage BX-51 microscope equipped with a 60X water immersion objective (Olympus Canada Inc, Richmond Hill, ON). Slices were perfused at 1.5 ml/min with warm oxygenated (95% O_2; 5% CO_2; 31.5 ± 1°C) artificial cerebrospinal fluid (ACSF). The ACSF comprised (in mM) NaCl (104), $NaHCO_3$ (26), NaH_2PO_4 (1.23), KCl (3), $MgCl_2$ (1), $CaCl_2$ (2), D-glucose (10), osmolality 297.5 ± 3 mosmol/kg. Where specified, bicuculline methochloride (Tocris, Oakville ON), tetrodotoxin (TTX) (Alomone Labs, Jerusalem) or mannitol (Fisher Scientific Co., Ottawa ON) were added into the ACSF.

All recordings were performed between 2:00 PM and 7:00 PM from cells identified as MNC^{VP} by the expression of eGFP. Patch pipettes were prepared from glass capillary tubes (1.2 mm o.d., AM Systems Inc.) filled will a solution containing (in mM) K-gluconate (110), HEPES (10), KCl (10), $MgCl_2$ (2) and Na-ATP (0.5). Pipette resistance in the bath was 3–4 MΩ and recordings where access resistance exceeded 25 MΩ were discarded.

Electrophysiology in slices—Current-clamp recordings obtained from identified MNC^{VP} in slices were performed without applying any holding current throughout the recording. Voltage-clamp recordings were performed with a holding voltage of −60 mV. In all slice experiments involving osmotic stimulation, a period of 10–12 minutes of stable baseline activity was followed by bath application of hyperosmotic ACSF (+15 mosmol/kg mannitol) for 10 minutes, itself followed by a 10-minute washout. Average values of action potential firing rate, membrane potential and sEPSC amplitude and frequency were determined from the final three minutes of the baseline and hypertonic stimulation periods. Membrane potential was determined from the peak of all-points histogram distributions (or average of all values in the segments analyzed) which reflects the brief stationary pauses between action potentials.

The amplitude and frequency of mEPSCs was determined during a 3 minute period recorded 5–10 min following establishment of the whole cell condition. Clampfit 10.0 software (Molecular Devices LLC, San Jose CA) was used to detect action potentials (threshold mode) and synaptic events (template mode).

To measure PPR and aEPSCs, a bipolar stimulating electrode made from twin Teflon-coated platinum wires (50 μm o.d.; A-M Systems Inc., Everett WA) was inserted into the OVLT and used to stimulate the local tissue. For PPR analysis two current pulses (1 ms, 50–100 μA; 50 ms apart) were delivered using an isolated stimulator. Charge transfer evoked during the two compound EPSCs was determined by integrating the current flowing during a period of 40 ms starting at the onset of each response, and PPR was calculated as the $EPSC_2/EPSC_1$ ratio. The average frequency and amplitude of aEPSCs was determined from events detected during the 250 ms that followed end of $EPSC_2$.

Acutely isolated MNCs—Isolated MNCs were prepared as previously described (Prager-Khoutorsky et al., 2014). Briefly, rats were sacrificed by decapitation, and the brain was rapidly removed and placed in chilled PIPES solution (~4°C; pH 7.3) containing (in mM): NaCl 120, KCl 5, $MgCl_2$ 1, PIPES 10, $CaCl_2$ 1 and glucose 10 (osmolality adjusted to 295 mosmol/kg using mannitol). Blocks of tissue containing the SON (~1 mm^3) were removed using iridectomy scissors and placed in PIPES solution containing 0.7 mg/ml protease XIV

(Sigma-Aldrich Canada Co., Oakville, ON) for 40 minutes. Tissue blocks were then transferred to protease-free PIPES solution, triturated using fire-polished Pasteur pipettes, and plated on 35 mm plastic Petri dishes. For live cell recording, imaging, or SICM analysis, dishes were placed on the stage of an IX-71 inverted phase-contrast microscope (Olympus Canada Inc.) and perfused with a HEPES-buffered saline solution (pH 7.3) containing (in mM): NaCl 140, KCl 3, $MgCl_2$ 1, HEPES 10, $CaCl_2$ 1, glucose 10; adjusted to 295 mosmol/kg with mannitol.

Electrophysiology in isolated MNCs—Recordings were performed between 2:00 PM and 7:00 PM from cells identified as MNC^{VP} by the expression of eGFP. Patch pipettes were prepared from glass capillary tubes (1.2 mm o.d., AM Systems Inc.) filled will a solution (pH 7.2) comprising (in mM): K-Gluconate 120, $MgCl_2$ 1, EGTA 10, HEPES 10, Na_2ATP 4, adjusted to 270 mosmol/kg. Pipette resistance in the bath was 3–6 MΩ and recordings where access resistance exceeded 25 MΩ were discarded. All cells were patch-clamped in the current-clamp mode. At the beginning of the recording a small amount of holding current was applied to the cell (0–5 pA) to adjust the initial voltage to a value near −70 mV and left unchanged for the remainder of the recording. After stable baseline activity was recorded for ~1 min, a ramp of negative pressure was applied to the pipette to provoke cell shrinking. The degree of cell shrinking evoked by negative pressure (expressed as percent change relative to control) was calculated from changes in maximal cross-sectional area (CSA) observed in control (CSA_0) and test conditions (CSA_t) using the equation; % shrinking = $100 \times [((CSA_0)^{1.5} – (CSA_t)^{1.5})/(CSA_0)^{1.5})]$ as previously described (Zhang and Bourque, 2003). For quantification, changes in membrane voltage, firing frequency, and cell volume were calculated as the average of values recorded during a 5 s segment centered on the frame used to calculate cell volume and compared to the average of values recorded during 20 s of baseline collected prior to the stimulus.

Analysis of membrane elasticity—Petri dishes containing MNCs acutely isolated from the SON and well rinsed with HEPES were placed in an Ionscope SICM with z axis resolution of 0.02 nm (Synoptics Ltd., Cambridge UK). Identified MNC^{VP} were approached in hopping mode with an 18 MΩ nano pipette probe filled with HEPES buffer. Hop height was set to 400 nm and fall rate was 5 nm/ms. Holding voltage was adjusted to achieve a holding current of ~700 pA and conductance decrease detection threshold set at 4–7%. The SICM controller keeps a constant distance between the tip of the nano probe and the cell surface using conductance-based feedback control of a piezo nanopositioner. This allows precision non-contact measurement of stress-strain (pressure-distance) curves to assess the elasticity of a living cell (Pellegrino et al., 2012; Sánchez et al., 2008). Once the cell surface was detected and locked in by the Ionscope controller, a ramp of positive pressure (P; ~100 mmHg at 2 mmHg/s) was applied to the pipette to apply a gradually increasing force against the surface membrane. The relative elasticity of the cell was expressed as the slope of the vertical displacement (Δz) observed as a function of P over the linear range of Δz/P values observed immediately upon increasing P. Cells were kept for analysis only if they showed ΔZ > 250 nm. One cell showing a value of Δz/P more than twice the standard deviation of the group was removed from the analysis.

Actin and tubulin staining—Isolated cells plated on Petri dishes were fixed for 30 minutes with phosphate buffered saline (PBS) containing 4% paraformaldehyde, then washed with PBS containing 0.25% Triton X-100. After 1–hour incubation with 2% normal goat serum diluted in PBS with 0.25% Triton, dishes were filled with PBS containing DM1A monoclonal anti-α-Tubulin diluted at 1:200 and incubated overnight at 4°C. Following wash, cells were incubated for 1 hour with goat anti-mouse secondary antibody (1:500; Thermo Fisher Scientific) conjugated to Alexa Fluor 647, then washed. For staining of F-actin, cells were exposed to Phalloidin conjugated to Alexa Fluor 568 (Thermo Fisher Scientific) diluted in PBS at 1:200 for 45 mins then washed. All images were acquired using a BX51 upright microscope (Olympus Canada Inc) equipped with a 60X water immersion objective and a Retiga R1 camera (Teledyne QImaging, Surrey BC). Image analysis was performed using ImageJ (https://imagej.nih.gov/ij/).

For analysis of subcortical F-actin, three straight analysis rectangles (approx. 92 × 10 pixels) were placed across the cell membrane approximately ~120° apart and peak subcortical intensity for each cell was determined as illustrated in Figure S2A. For α-tubulin, three circular regions of interest (ROI) were placed in the background and three other ROI were placed in the cytoplasmic region of the cell lying between the subcortical area and the perimeter of the nucleus. Average cytoplasmic α-tubulin intensity was determined as shown in Figure S2B.

QUANTIFICATION AND STATISTICAL ANALYSIS

All values in this study are reported as mean plus or minus the standard error of the mean (±s.e.m.). In each case normality of the data distribution was tested and the appropriate parametric or non-parametric tests were used to compare group values using Sigmaplot 12 software (SPSS Inc., Chicago IL). Differences between values were considered to be significant when $p < 0.05$. Graphs were prepared using either Sigmaplot 12, or Graphpad Prism (v.5). Linear regression analysis was performed using Sigmaplot 12.

Supplementary Material

Refer to Web version on PubMed Central for supplementary material.

ACKNOWLEDGMENTS

This work was supported by a James McGill Research Chair, a Canadian Institutes of Health Research (CIHR) Foundation grant (FDN-143337), and a grant from the Heart and Stroke Foundation of Canada (HSFC) to C.W.B. (G-16–00014197) and by grants from the National Institutes of Health (HL088052) and American Heart Association (15GNT25710176) to G.M.T. D.I.L. was supported by a CIHR Canada Graduate Scholarship Master's Award, J.C.W. was supported by a Grad Excellence Award in Neurology & Neurosurgery (M159875C51), and M.P.K. was supported by a HSFC National New Investigator Award. We thank Dr. Hal Gainer (NIH) for the generous supply of PS41 antibody and Dr. Thomas Cunningham (University of North Texas Health Sciences Centre at Fort Worth) for advice regarding statistical analysis of the c-fos data. The Research Institute of the McGill University Health Center receives generous support from Le Fonds de Recherche du Québec – Santé.

REFERENCES

Barad Z, Jacob-Tomas S, Sobrero A, Lean G, Hicks AI, Yang J, Choe KY, and Prager-Khoutorsky M (2020). Unique Organization of actin cytoskeleton in magnocellular vasopressin neurons in normal conditions and in response to salt-loading. eNeuro 7, ENEURO.0351–19.2020.

Basting T, Xu J, Mukerjee S, Epling J, Fuchs R, Sriramula S, and Lazartigues E (2018). Glutamatergic neurons of the paraventricular nucleus are critical contributors to the development of neurogenic hypertension. J. Physiol 596, 6235–6248. [PubMed: 30151830]

Bicknell RJ (1988). Optimizing release from peptide hormone secretory nerve terminals. J. Exp. Biol 139, 51–65. [PubMed: 2850339]

Boegehold MA (2002). Microvascular structure and function in salt-sensitive hypertension. Microcirculation 9, 225–241. [PubMed: 12152101]

Bourque CW (1991). Activity-dependent modulation of nerve terminal excitation in a mammalian peptidergic system. Trends Neurosci. 14, 28–30. [PubMed: 1709529]

Bourque CW (2008). Central mechanisms of osmosensation and systemic osmoregulation. Nat. Rev. Neurosci 9, 519–531. [PubMed: 18509340]

Brangwynne CP, MacKintosh FC, Kumar S, Geisse NA, Talbot J, Mahadevan L, Parker KK, Ingber DE, and Weitz DA (2006). Microtubules can bear enhanced compressive loads in living cells because of lateral reinforcement. J. Cell Biol 173, 733–741. [PubMed: 16754957]

Brown DR, Li SG, Lawler JE, and Randall DC (1999). Sympathetic control of BP and BP variability in borderline hypertensive rats on high- vs. low-salt diet. Am. J. Physiol 277, R650–R657. [PubMed: 10484480]

Cerrato BD, Frasch AP, Nakagawa P, Longo-Carbajosa N, Peña C, Höcht C, and Gironacci MM (2012). Angiotensin-(1–7) upregulates central nitric oxide synthase in spontaneously hypertensive rats. Brain Res. 1453, 1–7. [PubMed: 22483959]

Choe KY, Han SY, Gaub P, Shell B, Voisin DL, Knapp BA, Barker PA, Brown CH, Cunningham JT, and Bourque CW (2015). High salt intake increases blood pressure via BDNF-mediated downregulation of KCC2 and impaired baroreflex inhibition of vasopressin neurons. Neuron 85, 549–560. [PubMed: 25619659]

Chung L (2015). A Brief Introduction to the Transduction of Neural Activity into Fos Signal. Dev. Reprod 19, 61–67. [PubMed: 27004262]

Ciura S, and Bourque CW (2006). Transient receptor potential vanilloid 1 is required for intrinsic osmoreception in organum vasculosum lamina terminalis neurons and for normal thirst responses to systemic hyperosmolality. J. Neurosci 26, 9069–9075. [PubMed: 16943565]

Fink GD, Johnson RJ, and Galligan JJ (2000). Mechanisms of increased venous smooth muscle tone in desoxycorticosterone acetate-salt hypertension. Hypertension 35, 464–469. [PubMed: 10642342]

Fujita M, and Fujita T (2016). The Role of CNS in the Effects of Salt on Blood Pressure. Curr. Hypertens. Rep 18, 10. [PubMed: 26781250]

Gardel ML, Shin JH, MacKintosh FC, Mahadevan L, Matsudaira P, and Weitz DA (2004a). Elastic behavior of cross-linked and bundled actin networks. Science 304, 1301–1305. [PubMed: 15166374]

Gardel ML, Shin JH, MacKintosh FC, Mahadevan L, Matsudaira PA, and Weitz DA (2004b). Scaling of F-actin network rheology to probe single filament elasticity and dynamics. Phys. Rev. Lett 93, 188102. [PubMed: 15525211]

Gizowski C, and Bourque CW (2020). Sodium regulates clock time and output via an excitatory GABAergic pathway. Nature 583, 421–424. [PubMed: 32641825]

Gonzalez A, Moya-Alvarado G, Gonzalez-Billaut C, and Bronfman FC (2016). Cellular and molecular mechanisms regulating neuronal growth by brain-derived neurotrophic factor. Cytoskeleton 73, 612–628. [PubMed: 27223597]

Hicks AI, Barad Z, Sobrero A, Lean G, Jacob-Tomas S, Yang J, Choe KY, and Prager-Khoutorsky M (2020). Effects of salt loading on the organisation of microtubules in rat magnocellular vasopressin neurones. J. Neuroendocrinol 32, e12817. [PubMed: 31778225]

Ingber DE (2008). Tensegrity-based mechanosensing from macro to micro. Prog. Biophys. Mol. Biol 97, 163–179. [PubMed: 18406455]

Iremonger KJ, and Bains JS (2007). Integration of asynchronously released quanta prolongs the postsynaptic spike window. J. Neurosci 27, 6684–6691. [PubMed: 17581955]

Kannan H, and Yagi K (1978). Supraoptic neurosecretory neurons: evidence for the existence of coverging intpus both from carotid baroreceptors and osmoreceptors. Brain Res. 145, 385–390. [PubMed: 638798]

Keck T, Hübener M, and Bonhoeffer T (2017). Interactions between synaptic homeostatic mechanisms: an attempt to reconcile BCM theory, synaptic scaling, and changing excitation/inhibition balance. Curr. Opin. Neurobiol 43, 87–93. [PubMed: 28236778]

Kim JS, Kim WB, Kim YB, Lee Y, Kim YS, Shen FY, Lee SW, Park D, Choi HJ, Hur J, et al. (2011). Chronic hyperosmotic stress converts GABAergic inhibition into excitation in vasopressin and oxytocin neurons in the rat. J. Neurosci 31, 13312–13322. [PubMed: 21917814]

Kim YB, Kim YS, Kim WB, Shen FY, Lee SW, Chung HJ, Kim JS, Han HC, Colwell CS, and Kim YI (2013). GABAergic excitation of vasopressin neurons: possible mechanism underlying sodium-dependent hypertension. Circ. Res 113, 1296–1307. [PubMed: 24103391]

King AJ, and Fink GD (2006). Chronic low-dose angiotensin II infusion increases venomotor tone by neurogenic mechanisms. Hypertension 48, 927–933. [PubMed: 17000931]

King AJ, Osborn JW, and Fink GD (2007). Splanchnic circulation is a critical neural target in angiotensin II salt hypertension in rats. Hypertension 50, 547–556. [PubMed: 17646575]

Kinsman BJ, Browning KN, and Stocker SD (2017a). NaCl and osmolarity produce different responses in organum vasculosum of the lamina terminalis neurons, sympathetic nerve activity and blood pressure. J. Physiol 595, 6187–6201. [PubMed: 28678348]

Kinsman BJ, Nation HN, and Stocker SD (2017b). Hypothalamic Signaling in Body Fluid Homeostasis and Hypertension. Curr. Hypertens. Rep 19, 50. [PubMed: 28528375]

Kinsman BJ, Simmonds SS, Browning KN, and Stocker SD (2017c). Organum Vasculosum of the Lamina Terminalis Detects NaCl to Elevate Sympathetic Nerve Activity and Blood Pressure. Hypertension 69, 163–170. [PubMed: 27895193]

Kuroki MT, Guzman PA, Fink GD, and Osborn JW (2012). Time-dependent changes in autonomic control of splanchnic vascular resistance and heart rate in ANG II-salt hypertension. Am. J. Physiol. Heart Circ. Physiol 302, H763–H769. [PubMed: 22114134]

Leng G, Brown CH, Bull PM, Brown D, Scullion S, Currie J, Blackburn-Munro RE, Feng J, Onaka T, Verbalis JG, et al. (2001). Responses of magnocellular neurons to osmotic stimulation involves coactivation of excitatory and inhibitory input: an experimental and theoretical analysis. J. Neurosci 21, 6967–6977. [PubMed: 11517284]

Malta D, Petersen KS, Johnson C, Trieu K, Rae S, Jefferson K, Santos JA, Wong MMY, Raj TS, Webster J, et al. (2018). High sodium intake increases blood pressure and risk of kidney disease. From the Science of Salt: A regularly updated systematic review of salt and health outcomes (August 2016 to March 2017). J. Clin. Hypertens 20, 1654–1665.

McBryde FD, Guild SJ, Barrett CJ, Osborn JW, and Malpas SC (2007). Angiotensin II-based hypertension and the sympathetic nervous system: the role of dose and increased dietary salt in rabbits. Exp. Physiol 92, 831–840. [PubMed: 17468201]

Nissen R, Bourque CW, and Renaud LP (1993). Membrane properties of organum vasculosum lamina terminalis neurons recorded in vitro. Am. J. Physiol 264, R811–R815. [PubMed: 8476124]

Nomura K, Hiyama TY, Sakuta H, Matsuda T, Lin CH, Kobayashi K, Kobayashi K, Kuwaki T, Takahashi K, Matsui S, and Noda M (2019). [Na^+] Increases in Body Fluids Sensed by Central Na_x Induce Sympathetically Mediated Blood Pressure Elevations via H^+-Dependent Activation of ASIC1a. Neuron 101, 60–75.e6. [PubMed: 30503172]

Osborn JW, Fink GD, Sved AF, Toney GM, and Raizada MK (2007). Circulating angiotensin II and dietary salt: converging signals for neurogenic hypertension. Curr. Hypertens. Rep 9, 228–235. [PubMed: 17519130]

Ozaki Y, Soya A, Nakamura J, Matsumoto T, and Ueta Y (2004). Potentiation by angiotensin II of spontaneous excitatory postsynaptic currents in rat supraoptic magnocellular neurones. J. Neuroendocrinol 16, 871–879. [PubMed: 15584928]

Palmer BF (2015). Vasopressin receptor antagonists. Curr. Hypertens. Rep 17, 510. [PubMed: 25604388]

Panatier A, Gentles SJ, Bourque CW, and Oliet SH (2006). Activity-dependent synaptic plasticity in the supraoptic nucleus of the rat hypothalamus. J. Physiol 573, 711–721. [PubMed: 16613872]

Pellegrino M, Pellegrini M, Orsini P, Tognoni E, Ascoli C, Baschieri P, and Dinelli F (2012). Measuring the elastic properties of living cells through the analysis of current-displacement curves in scanning ion conductance microscopy. Pflugers Arch. 464, 307–316. [PubMed: 22744227]

Prager-Khoutorsky M, and Bourque CW (2010). Osmosensation in vasopressin neurons: changing actin density to optimize function. Trends Neurosci. 33, 76–83. [PubMed: 19963290]

Prager-Khoutorsky M, and Bourque CW (2015). Mechanical basis of osmosensory transduction in magnocellular neurosecretory neurones of the rat supraoptic nucleus. J. Neuroendocrinol 27, 507–515. [PubMed: 25712904]

Prager-Khoutorsky M, Khoutorsky A, and Bourque CW (2014). Unique interweaved microtubule scaffold mediates osmosensory transduction via physical interaction with TRPV1. Neuron 83, 866–878. [PubMed: 25123313]

Prager-Khoutorsky M, Choe KY, Levi DI, and Bourque CW (2017). Role of Vasopressin in Rat Models of Salt-Dependent Hypertension. Curr. Hypertens. Rep 19, 42. [PubMed: 28451854]

Richard D, and Bourque CW (1995). Synaptic control of rat supraoptic neurones during osmotic stimulation of the organum vasculosum lamina terminalis in vitro. J. Physiol 489, 567–577. [PubMed: 8847648]

Sánchez D, Johnson N, Li C, Novak P, Rheinlaender J, Zhang Y, Anand U, Anand P, Gorelik J, Frolenkov GI, et al. (2008). Noncontact measurement of the local mechanical properties of living cells using pressure applied via a pipette. Biophys. J 95, 3017–3027. [PubMed: 18515369]

Sharif Naeini R, Witty MF, Séguéla P, and Bourque CW (2006). An N-terminal variant of Trpv1 channel is required for osmosensory transduction. Nat. Neurosci. 9, 93–98. [PubMed: 16327782]

Shi P, Stocker SD, and Toney GM (2007). Organum vasculosum laminae terminalis contributes to increased sympathetic nerve activity induced by central hyperosmolality. Am. J. Physiol. Regul. Integr. Comp. Physiol 293, R2279–R2289. [PubMed: 17898124]

Shin JH, Gardel ML, Mahadevan L, Matsudaira P, and Weitz DA (2004). Relating microstructure to rheology of a bundled and cross-linked F-actin network in vitro. Proc. Natl. Acad. Sci. USA 101, 9636–9641. [PubMed: 15210969]

Son SJ, Filosa JA, Potapenko ES, Biancardi VC, Zheng H, Patel KP, Tobin VA, Ludwig M, and Stern JE (2013). Dendritic peptide release mediates interpopulation crosstalk between neurosecretory and preautonomic networks. Neuron 78, 1036–1049. [PubMed: 23791197]

Stachniak TJ, Trudel E, and Bourque CW (2014). Cell-specific retrograde signals mediate antiparallel effects of angiotensin II on osmoreceptor afferents to vasopressin and oxytocin neurons. Cell Rep. 8, 355–362. [PubMed: 25043186]

Sudbury JR, Ciura S, Sharif-Naeini R, and Bourque CW (2010). Osmotic and thermal control of magnocellular neurosecretory neurons–role of an N-terminal variant of trpv1. Eur. J. Neurosci 32, 2022–2030. [PubMed: 21143657]

Toney GM, and Stocker SD (2010). Hyperosmotic activation of CNS sympathetic drive: implications for cardiovascular disease. J. Physiol 588, 3375–3384. [PubMed: 20603334]

Trudel E, and Bourque CW (2003). A rat brain slice preserving synaptic connections between neurons of the suprachiasmatic nucleus, organum vasculosum lamina terminalis and supraoptic nucleus. J. Neurosci. Methods 128, 67–77. [PubMed: 12948549]

Trudel E, and Bourque CW (2010). Central clock excites vasopressin neurons by waking osmosensory afferents during late sleep. Nat. Neurosci 13, 467–474. [PubMed: 20190744]

Ueta Y, Fujihara H, Serino R, Dayanithi G, Ozawa H, Matsuda K, Kawata M, Yamada J, Ueno S, Fukuda A, and Murphy D (2005). Transgenic expression of enhanced green fluorescent protein enables direct visualization for physiological studies of vasopressin neurons and isolated nerve terminals of the rat. Endocrinology 146, 406–413. [PubMed: 15375027]

Vivas L, Chiaraviglio E, and Carrer HF (1990). Rat organum vasculosum laminae terminalis in vitro: responses to changes in sodium concentration. Brain Res. 519, 294–300. [PubMed: 2397412]

Xu H, Fink GD, and Galligan JJ (2007). Increased sympathetic venoconstriction and reactivity to norepinephrine in mesenteric veins in anesthetized DOCA-salt hypertensive rats. Am. J. Physiol. Heart Circ. Physiol. 293, H160–H168. [PubMed: 17322411]

Zaelzer C, Hua P, Prager-Khoutorsky M, Ciura S, Voisin DL, Liedtke W, and Bourque CW (2015). DN-TRPV1: A Molecular Co-detector of Body Temperature and Osmotic Stress. Cell Rep. 13, 23–30. [PubMed: 26387947]

Zhang Z, and Bourque CW (2003). Osmometry in osmosensory neurons. Nat. Neurosci 6, 1021–1022. [PubMed: 12973356]

Zhang Z, and Bourque CW (2008). Amplification of transducer gain by angiotensin II-mediated enhancement of cortical actin density in osmosensory neurons. J. Neurosci 28, 9536–9544. [PubMed: 18799685]

Zhang Z, Kindrat AN, Sharif-Naeini R, and Bourque CW (2007). Actin filaments mediate mechanical gating during osmosensory transduction in rat supraoptic nucleus neurons. J. Neurosci 27, 4008–4013. [PubMed: 17428977]

Zucker RS, and Regehr WG (2002). Short-term synaptic plasticity. Annu. Rev. Physiol 64, 355–405. [PubMed: 11826273]

Highlights

- High dietary salt increases the osmoresponsiveness of vasopressin neurons *in vivo*
- Salt loading and AngII-salt both increase the mEPSC amplitude in vasopressin neurons
- AngII-salt increases glutamate release probability and overall network excitation
- Salt loading increases stiffness and intrinsic osmosensitivity of vasopressin neurons

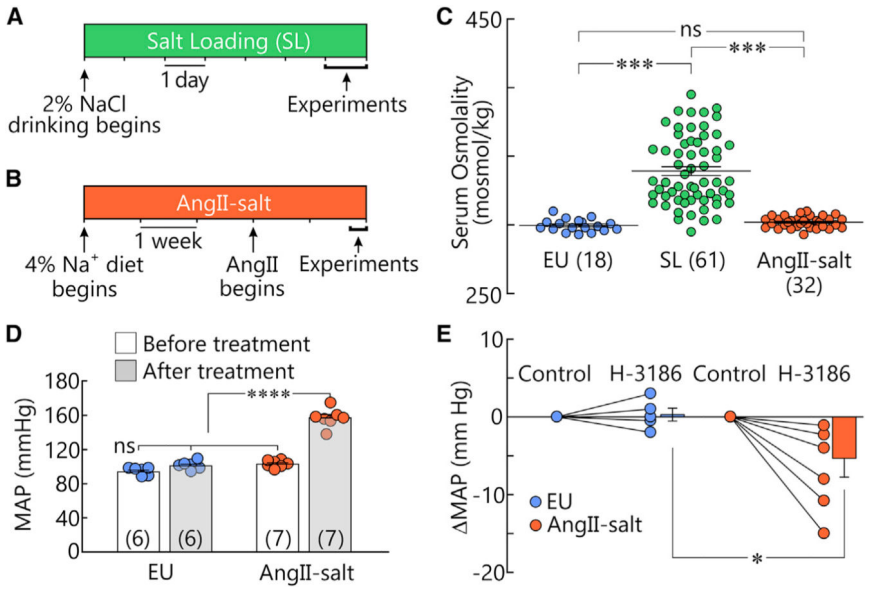

Figure 1. Two models of salt-dependent hypertension

(A and B) Graphical representation of the treatments used for SL (A) and AngII-salt (B).

(C) Distribution of values of serum osmolality measured in rats subjected to EU, SL, or AngII-salt. Lines representing mean and SEM values are superimposed on the samples. ***$p < 0.001$; ns, not significant.

(D) Bar graphs show mean ± SEM MAP recorded by telemetry in freely moving rats before and after AngII-salt treatment or at a corresponding time interval in EU rats (n shown in brackets). ****$p < 0.0001$.

(E) Graph shows changes in MAP induced by H-3186 relative to baseline (Control) in animals subjected to EU or AngII-salt (2 point plots) and mean ± SEM changes in MAP in the same groups (bar graphs). *$p < 0.05$.

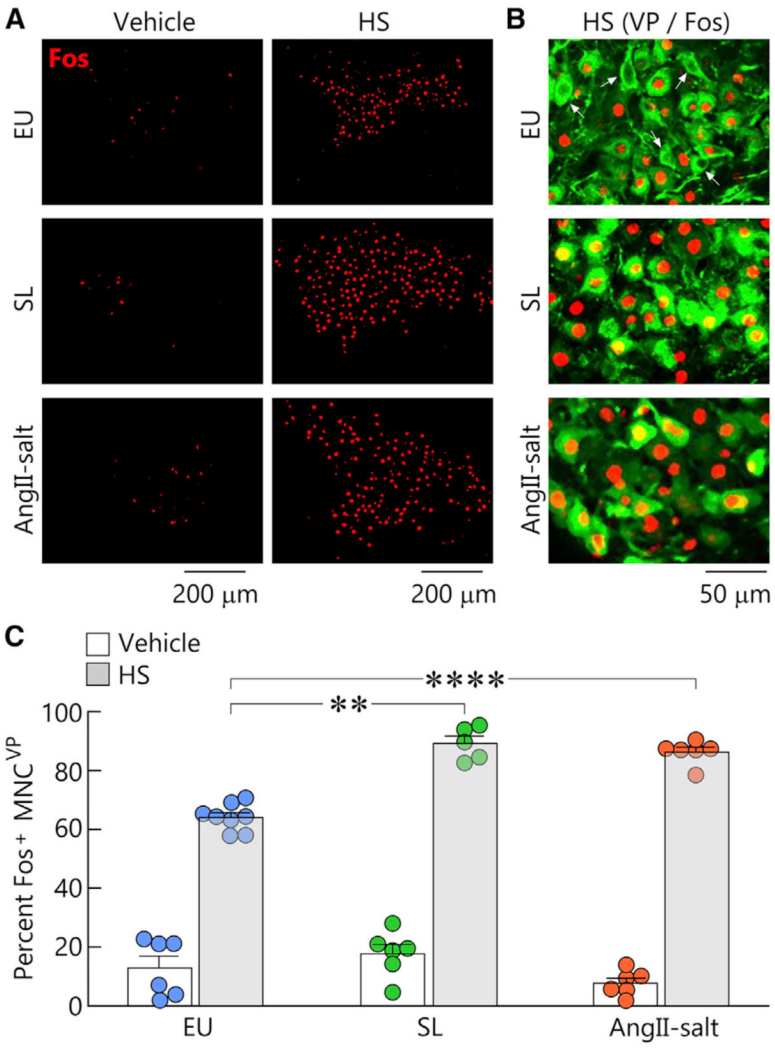

Figure 2. AngII-salt and SL sensitize osmoresponsiveness of MNC^{VP} *in vivo*

(A) Micrographs are confocal images of c-*fos* (Fos, red) immunoreactivity in the SON of EU, SL, and AngII-salt rats that were injected with either vehicle or hypertonic saline (HS). Scale bars 200 μm.

(B) Higher-power confocal images showing Fos in MNC^{VP} (green) in HS-treated animals for all treatments. Note the presence of Fos-negative MNC^{VP} in HS-treated EU. Scale bar 50 μm.

(C) Bar graphs show mean ± SEM percentage (%) of MNC^{VP} that were Fos positive (Fos^{+}) in all conditions. Each circle represents the average percentage determined by analysis of 2–4 sections in each rat tested. **p < 0.01, ****p < 0.001.

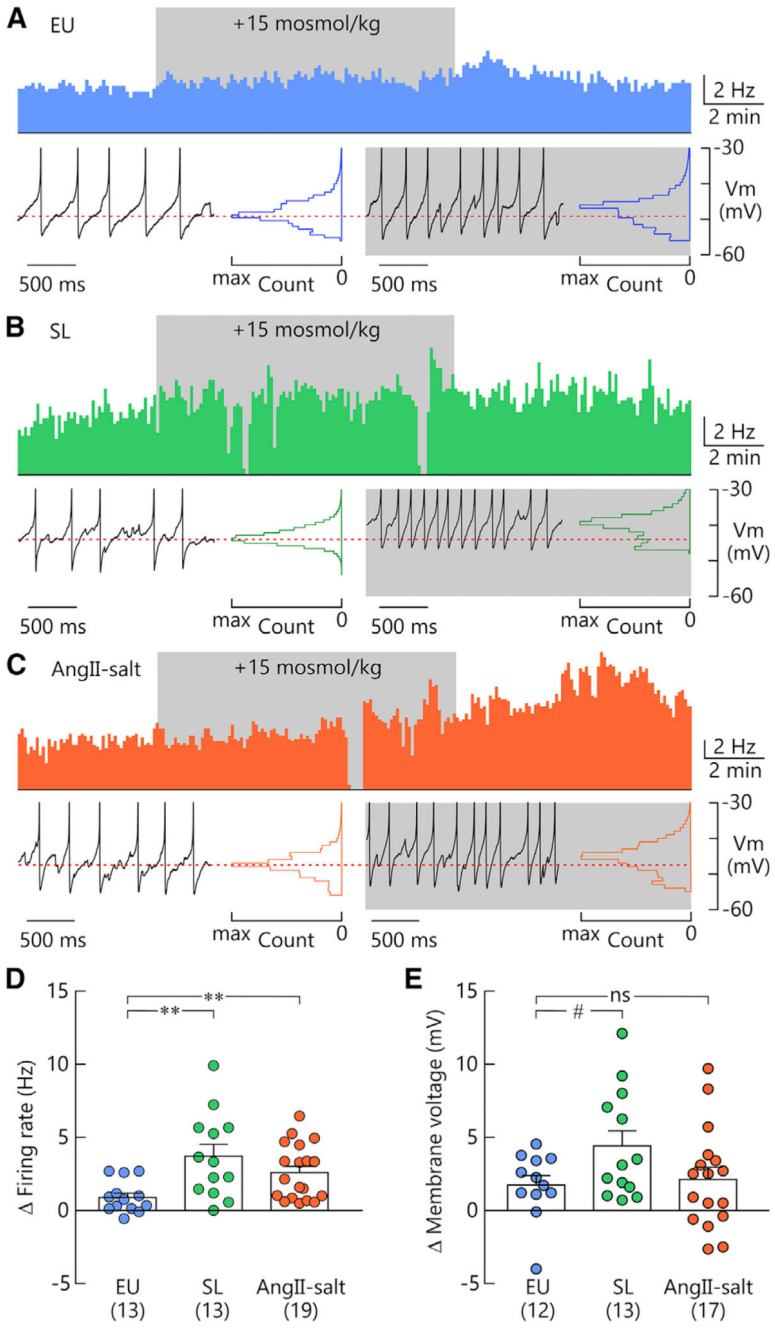

Figure 3. SL and AngII-salt increase osmoresponsiveness of MNC^{VP} *in vitro*

(A–C) Top: histograms show action potential firing rate of current-clamped MNC^{VP} in brain slices from EU (A), SL (B), and AngII-salt (C) animals. Gray areas indicate where a hyperosmotic stimulus was applied (+15 mosmol/kg mannitol). Bottom: traces are excerpts from the recording and corresponding all-points voltage histograms obtained in the absence and presence (gray) of the hyperosmotic stimulus in EU (A), SL (B), and AngII-salt (C). Dashed lines show membrane potential in isotonic conditions.

(D) Bar graphs show mean ± SEM changes in firing rate induced by hyperosmolality in MNC^{VP} recorded in slices from 9 EU, 10 SL, and 10 AngII-salt animals (each dot is data from a different cell, n shown in brackets). **$p < 0.01$.

(E) Bar graphs show mean ± SEM changes in membrane voltage induced by a +15 mosmol/kg hyperosmotic stimulus in MNC^{VP} recorded in horizontal brain slices obtained from 9 EU, 10 SL, and 9 AngII-salt rats. #$p < 0.05$ by t test.

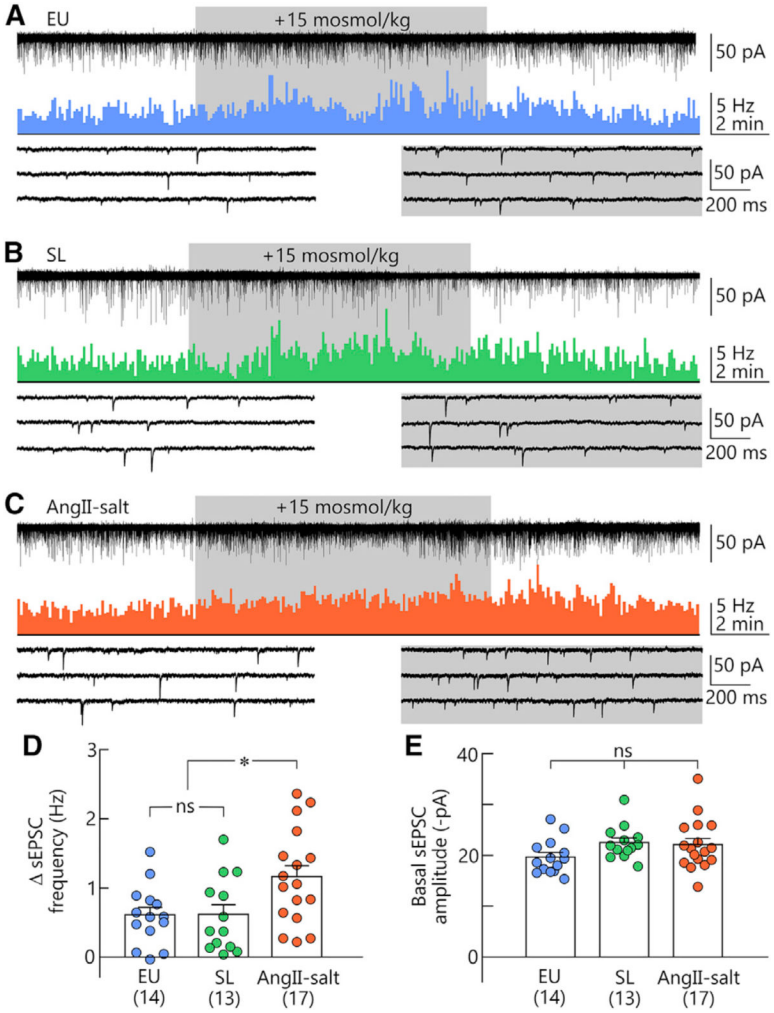

Figure 4. AngII-salt potentiates osmotically induced synaptic excitation in MNC^{VP}

(A–C) Top: gap-free membrane current recording (top) and corresponding sEPSC frequency histogram (bottom) showing the effect of a hyperosmotic stimulus (+15 mosmol/kg, gray area) on voltage-clamped MNC^{VP} (V_h = −60 mV) in horizontal brain slices obtained from EU (A), SL (B), and AngII-salt animals (C). Bicuculline (5 μM) was present throughout. Bottom: representative excerpts showing sEPSCs in the basal conditions and in presence of a hyperosmotic stimulus (gray area).

(D) Bar graphs show mean ± SEM hypertonicity-induced changes in sEPSC frequency recorded in MNC^{VP} in slices obtained from 8 EU, 5 SL, and 7 AngII-salt animals. Each dot is data from a different cell, n shown in brackets. *$p < 0.05$, ns, not statistically significant.

(E) Bar graphs show mean ± SEM amplitudes of sEPSCs recorded under basal conditions from MNC^{VP} in slices obtained from 8 EU, 5 SL, and 7 AngII-salt animals.

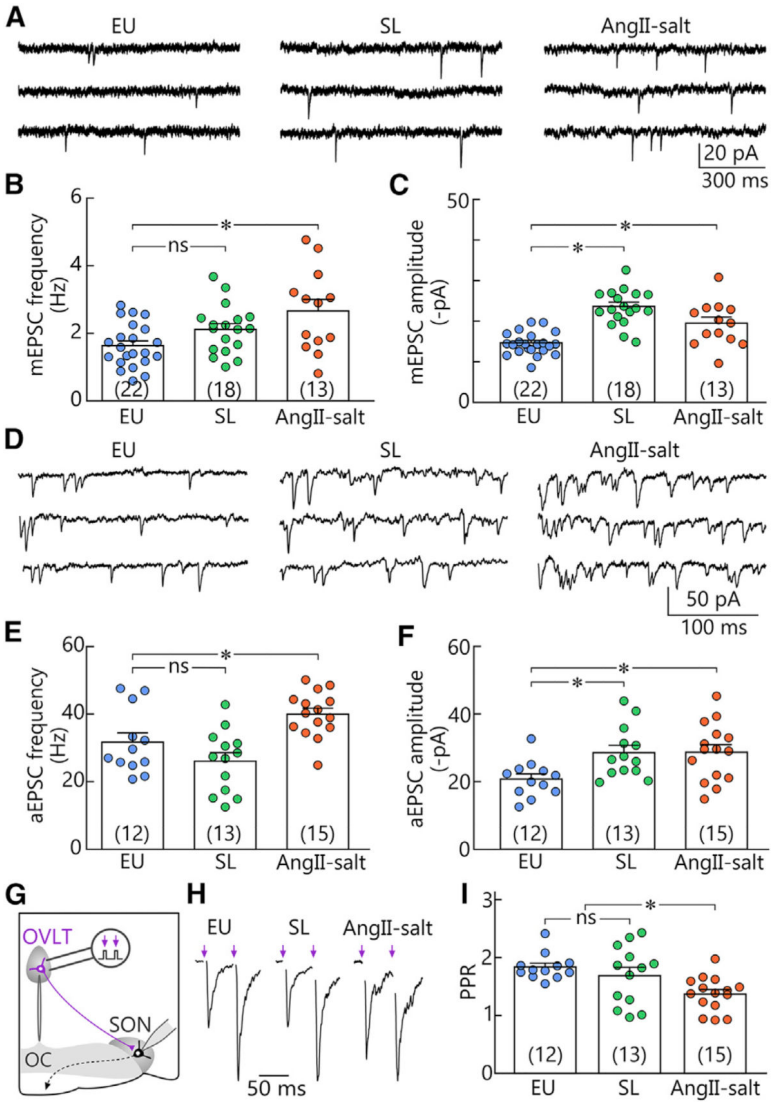

Figure 5. Effect of SL and AngII-salt on glutamate synapses in MNC^{VP}

(A) Representative traces showing miniature EPSCs (mEPSCs; ACSF contains1 μM TTX and 5 μM bicuculline) recorded from MNC^{VP} in horizontal brain slices from EU, SL, and AngII-salt animals.

(B) Bar graphs show mean ± SEM mEPSC frequency in MNC^{VP} from 4 EU, 5 SL, and 2 AngII-salt animals. Each dot is data from a different cell.

(C) Bar graphs show mean ± SEM mEPSC amplitudes in MNC^{VP} from 4 EU, 5 SL, and 2 AngII-salt animals.

(D) Representative current traces showing asynchronous EPSCs (aEPSCs) recorded from MNC^{VP} in slices from EU, SL, and AngII-salt animals.

(E) Bar graphs show mean ± SEM aEPSC frequency in MNC^{VP} in slices from 3 EU, 3 SL, and 4 AngII-salt animals.

(F) Bar graphs show mean ± SEM aEPSC amplitudes in MNC^{VP} in slices from 3 EU, 3 SL, and 4 AngII-salt animals.

(G) Schematic illustrating paired-pulse analysis of OVLT→SON synapses in MNC^{VP}.

(H) Three representative traces show pairs of EPSCs evoked by electrical stimuli delivered to the OVLT 50 ms apart (purple arrows). Recordings are from MNC^{VP} in slices prepared from EU, SL, and AngII-salt animals.

(I) Bar graphs show mean ± SEM values of the paired pulse ratio (PPR) recorded in MNC^{VP} from 3 EU, 3 SL, and 4 AngII-salt animals. *$p < 0.05$; ns not statistically significant.

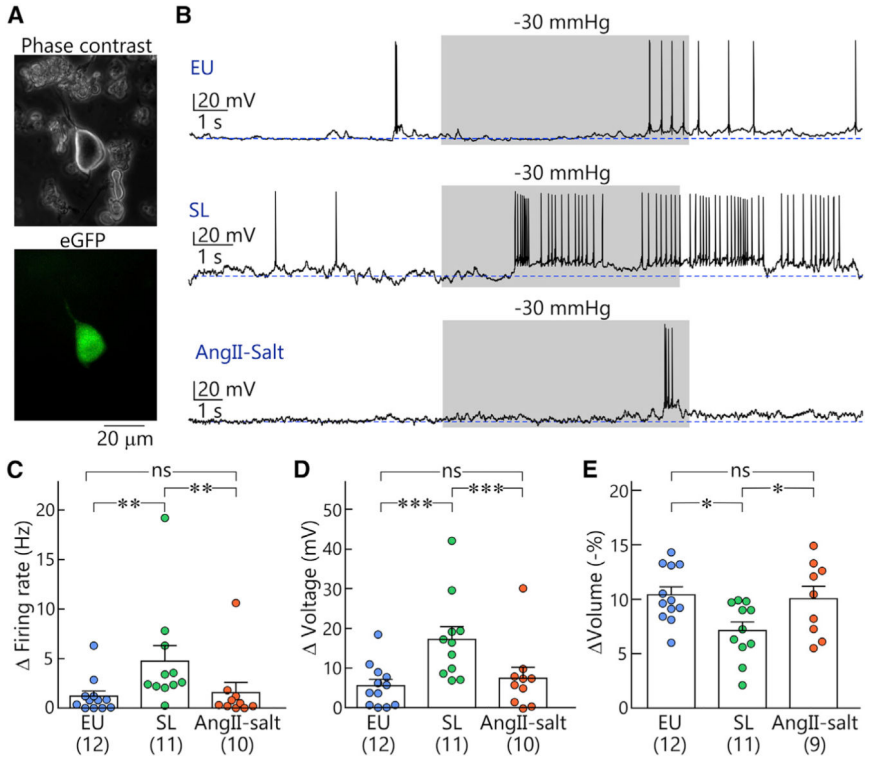

Figure 6. Mechanosensitivity of MNC^{VP} isolated from EU, SL, and AngII-salt rats

(A) Phase-contrast (top) and eGFP fluorescence(bottom) images of an acutely isolated MNC^{VP}. Scale bar 20 µm.

(B) Traces are representative whole-cell voltage recordings showing the effects of shrinking induced by application of negative pressure (−30 mmHg) to the patch electrode on cells from EU, SL, and AngII-salt animals. Dashed line extends the baseline voltage recorded before the stimulus was applied.

(C) Bar graphs show mean ± SEM changes in action potential firing rate induced by negative pressure in MNC^{VP} isolated from EU, SL, and AngII-salt rats (each dot is data from a different cell; n shown in brackets).

(D) Bar graphs show mean ± SEM changes in voltage induced by negative pressure in MNC^{VP} isolated from EU, SL, and AngII-salt rats.

(E) Bar graphs show mean ± SEM changes in soma volume induced by negative pressure in MNC^{VP} isolated from EU, SL, and AngII-salt rats. Changes are expressed as percentage decrease (−%) relative to baseline volume. *$p < 0.05$, **$p < 0.01$, ***$p < 0.005$.

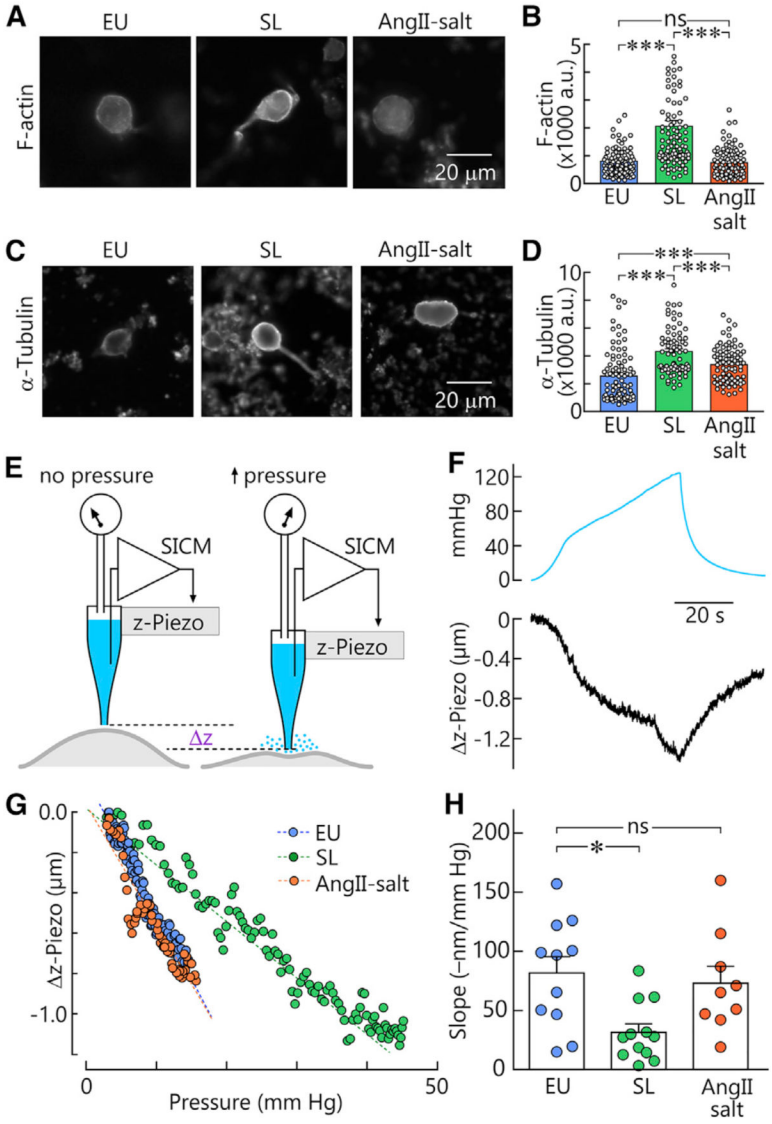

Figure 7. SL increases stiffness of MNC^{VP}

(A) Micrographs show fluorescent phalloidin (F-actin) in MNC^{VP} isolated from EU, SL, and AngII-salt rats. Scale bar 20 μm.

(B) Bar graphs show mean ± SEM subcortical F-actin intensity in arbitrary units (a.u.) in MNC^{VP} in all conditions (each dot is data from a different cell).

(C) Micrographs show fluorescently labeled α-tubulin in MNC^{VP} isolated from EU, SL, and AngII-salt rats. Scale bar 20 μm.

(D) Bar graphs show mean ± SEM perinuclear cytoplasmic fluorescence intensity in all conditions.

(E) Schematic of a cell-rigidity assay with scanning ion conductance microscopy (SICM). The pipette nanoprobe (blue) is placed orthogonal to the cell surface, and the vertical position is continuously maintained at a constant distance from the membrane through resistance-based feedback control by the SICM. The z position is monitored by a high-

resolution piezo (z-Piezo) as positive pressure is applied to cause the cell surface to flex inward.

(F) Plots show an example of the change in z-Piezo position achieved as pressure in the pipette is increased.

(G) Plots show examples of changes in z-Piezo position (Δz-Piezo) associated with increasing pipette pressure in cells from EU, SL, and AngII-salt animals. Dashed lines are linear regression fits of the data to obtain slope values.

(H) Bar graphs show mean ± SEM slope values measured in MNC^{VP} isolated from EU, SL, and AngII-salt rats. *$p < 0.05$, ***$p < 0.005$.

KEY RESOURCES TABLE

REAGENT or RESOURCE	SOURCE	IDENTIFIER
Antibodies		
Rabbit anti-fos polyclonal	Millipore (Billerica MA)	N/A
Rabbit anti-fos polyclonal	SYSY	Cat: 226003;RRID:AB_2231974
Mouse anti-VP-neurophysin monoclonal	Hal Gainer, NIH	PS-41
Mouse anti-alpha-tubulin monoclonal	Sigma	DM1A: T6199; RRID:AB_477583
Alexa-405 anti-rabbit IGG secondary	Invitrogen	Cat: A-31556; RRID:AB_221605
Alexa-568 anti-mouse IGG secondary	Invitrogen	Cat: A-11031; RRID:AB_144696
Alexa-647 anti-mouse IGG secondary	Invitrogen	Cat: A-21235; RRID:AB_2535804
Chemicals, peptides, and recombinant proteins		
Tetrodotoxin	Affix Scientific	Cas: AF3015
Bicuculline methochloride	Tocris	Cas: 53552-05-9
Protease XIV	Sigma-Aldrich	Cas:9036-06-0
Phalloidin-congugated-Alexa 568	Invitrogen	Cat: A12380
H-3186 (AVP receptor 1 antagonist)	Bachem	4031343.0001
Angiotensin II	Sigma-Aldrich	Cas:4474-91-3
Experimental models: organisms/strains		
AVP-eGFP Wistar transgenic rats	Yoichi Ueta, University of environmental and occupational health, Kitakyushu Japan	N/A
Software and algorithms		
Sigmaplot 12	SPSS Inc	N/A
Prism 5	Graphpad	N/A
Clampfit 10	Molecular Devices	N/A
SICM Ionoscope Part 00201	Open iO Labs	N/A
FIJI (ImageJ)	N.I.H.	https://imagej.net/Fiji
Retiga R6 imaging software	QImaging	Occular
Confocal Imaging software	Olympus Canada	FV31S-SW
Other		
Osmotic minipumps	Alzet	0000325
Salt Chow	Research Diets, Inc.	D17013i
Osmometer	Advanced Instruments	Model 3320